J Mater Sci: Mater Electron (2017) 28:1472–1479
DOI 10.1007/s10854-016-5683-y

Annealing atmosphere dependant properties of biosynthesized TiO_2 anode for lithium ion battery application

Anil A. Kashale[1] · Kalyani A. Ghule[1] · Ketan P. Gattu[1] · Vijay H. Ingole[1] · Swapnali S. Dhanayat[1] · Ramphal Sharma[1] · Yong-Chien Ling[2] · Jia-Yaw Chang[3] · Madagonda M. Vadiyar[4] · Anil Vithal Ghule[1,2,4]

Received: 5 July 2016 / Accepted: 2 September 2016 / Published online: 7 September 2016

Abstract The present work demonstrates the synthesis of in situ carbon incorporated TiO_2 nanoparticles (Bio-TiO_2/C) and bare Bio-TiO_2 from low cost and eco-friendly materials, wherein Bengal gram beans (*Cicer arietinum* L.) extract containing bio-molecules is used as complexing agent to stabilize and engineer Bio-TiO_2/C used as anode for lithium ion battery application. The influence of annealing atmosphere (argon and air) on the formation of carbon anchored biosynthesized TiO_2 nano-spheres is investigated systematically. Interestingly, selective formation of TiO_2/C nano-spheres is observed in argon atmosphere, while annealing in air leads to the formation of carbon free TiO_2 nanoparticles. The gram bean extract containing biomass helps to inhibit the aggregation, leading to uniform size distribution of TiO_2 nanoparticles. These biomasses convert into carbon after calcination of as prepared Bio-TiO_2 in argon atmosphere (Bio-TiO_2/C), and in air calcinations, these biomasses are completely oxidised and form bare Bio-TiO_2. The resulting products TiO_2/C and TiO_2 are characterized using thermogravimetry analyzer, X-ray diffraction, transmission electron microscopy, Raman spectrophotometer, X-ray photoelectron spectroscopy and Fourier transform infrared spectroscopy. Furthermore, the prepared TiO_2/C and TiO_2 are investigated as electrodes for lithium ion battery. The charge/discharge performance of TiO_2/C shows an initial reversible capacity of 208 mA h g^{-1} at a current density of 33 mA g^{-1}, which is higher than TiO_2 nanoparticles (197 mA h g^{-1}). The cycling study exhibit TiO_2/C based electrode retaining about 100 % of reversible capacity after 60 cycles at same current density, which is 3 % higher than the TiO_2 nanoparticles based electrode.

1 Introduction

Lithium-ion batteries (LIBs) are one among the smart energy storage systems and have increasing commercial demand in rechargeable power sources for various consumer electronic equipments and electric and hybrid cars, owing to their unique features like lightweight, smaller, environmental friendly, high energy density, fast charge/discharge rate, excellent cycle performance and fully rechargeable [1–6]. Although, LIBs have attractive properties compared to conventional primary batteries, their electrochemical properties still have been largely restricted by electrode materials. Anode is one of the most important and key factors for improving the electrochemical performance and service. To date, generally carbonaceous (graphite) materials are being used in commercial LIBs [7, 8]. However, these LIBs have serious issues related to safety and rate performance as the carbonaceous electrode material suffer from lithium dendrite on the surface of electrodes [9]. Thus, alternative transition metal oxides as anode materials are being explored with great interest to

✉ Anil Vithal Ghule
anighule@gmail.com

Jia-Yaw Chang
jychang@mail.ntust.edu.tw

[1] Department of Nanotechnology, Dr. Babasaheb Ambedkar Marathwada University, Aurangabad, Maharashtra 431004, India

[2] Department of Chemistry, National Tsing Hua University, Hsinchu 30013, Taiwan

[3] Department of Chemical Engineering, National Taiwan University of Science and Technology, Taipei 10607, Taiwan

[4] Department of Chemistry, Shivaji University, Kolhapur, Maharashtra 416004, India

circumvent these problems. Transition metal oxides like SnO_2 [10, 11], NiO [12, 13], Co_3O_4 [14], $ZnFe_2O_4$ [15] Fe_2O_3 [16], Cr_2O_3 [17] and TiO_2 [18, 19] have attracted significant attention of the research community for lithium storage devices due to their stable reversibility and enhanced security capability. Among the explored transition metal oxides, titanium dioxide is considered as one of the most appreciable and an alternative anode material because of its abundant and low cost sources, easy availability, environmentally benignity and high chemical stability. Besides, titanium dioxide can operate at higher working potential, which help prevent lithium dendrite formation on the electrode surfaces. Apart from this, the volume change ($\sim$4 %) during charging-discharging is relatively very low accounting for good structural stability [20–22]. Titanium dioxide is present in nature in four common forms: anatase, rutile, brookite and TiO_2(B). Among these polymorphs, anatase TiO_2 has been investigated as promising prospective electrode material because of its special crystal structure providing abundant accessible channels for fast lithium-ion transport. However, the intrinsic poor electronic conductivity and ionic conductivity has hampered its use as electrode material in LIBs [23, 24].

Partially, some of these issues have been circumvented by combining TiO_2 with various carbon materials such as amorphous carbon, carbon fibres, graphene, carbon nanotubes etc. [25, 26]. Goriparti et al. [27] prepared carbon doped TiO_2 nanowires and demonstrated their increasing electrochemical performance by decreasing the Li-ion diffusion length, which improved the electrical conductivity of the nanowires. Chen et al. [28] synthesized carbon incorporated titanium dioxide for improving the reversibility and long-term cycling capability, which is attributed to the inherently incorporated carbon species efficiently improving electronic conductivity. Similarly, Chen et al. [19] synthesized carbon-coated anatase TiO_2 nanoparticles (CTON; PVDF) and noted enhanced rate performance as a result of carbon coating, which improved electrical conductivity. On the other hand, Wang et al. [29] fabricated hybrid TiO_2–carbon materials and observed significantly enhanced Li-ion insertion/extraction in TiO_2. Numerous synthesis techniques for example, hydrothermal, sol–gel, electrodeposition, evaporation induced self-assembly and application of ionic liquids with different type of carbon sources (sucrose, ethanol, PVDF, polyacrylonitrile, cellulose, CNTs and acetic acid) have been proposed to synthesize titanium dioxide and its oxide–carbon composite [26, 30, 31].

Considering the issues related to both graphite and TiO_2 in the field of lithium ion battery, trying to tackle the problem of conductivity of TiO_2 by incorporating the carbon through in situ synthesis of TiO_2 is promising. Furthermore, incorporating carbon in TiO_2 using bio-green synthesis approach is relatively less explored. Thus, with this motivation, herein this work, bio-mediated synthesis of in situ carbon incorporated TiO_2 nanoparticles (Bio-TiO_2/C) is reported, wherein, gram beam extract (remnant water of Bengal gram bean) containing bio-molecules (Pectin), which act as a bulky capping agent help in stabilizing the titanium ions and hinder aggregation of titanium oxide nanoparticles and also function as ideal source of carbon. This in situ incorporated carbon in TiO_2 helps to increase the electrical conductivity and diffusion coefficient of Li ion in the structure. The gram bean extract containing biomass helps to inhibit the aggregation leading to uniform size distribution of TiO_2 nanoparticles and these biomasses convert into carbon after calcination of as prepared Bio-TiO_2 in argon atmosphere (Bio-TiO_2/C) and in air calcination these biomasses are completely oxidised and form bare Bio-TiO_2. Further characterization of biosynthesized TiO_2 nanoparticles (Bio-TiO_2/C and Bio-TiO_2) and investigation of their electrochemical performance for Li ion battery application is carried out.

2 Experimental procedure

2.1 Chemicals

Dry Bengal gram beans (*Cicer arietinum* L.) were obtained from local market in Aurangabad, India. $TiCl_4$ and ammonia (AR grade 28 %) purchased from Merck were used as such without further purification.

2.2 Bio-TiO_2/C composite nanoparticles using gram bean extract

The procedure for synthesis of Bio-TiO_2/C nanoparticles is similar to our previous report for SnO_2 synthesis, except for the precursor [32–34]. In typical synthesis, 20 g of dry Bengal gram beans (*C. arietinum* L.) were soaked in 100 mL DI water for 6 h at room temperature (25 °C). Thereafter, the soaked seeds were removed and the extract was filtrated using a glass-fiber filter (GF/F) to be free from particulate matter. 10 mL of $TiCl_4$ solution was added to 10 mL of the gram bean extract and diluted to 50 mL. The ammonia is added in the diluted solution to make pH of the solution to 7 and was stirred for 1 h for the formation of titanium hydroxide-pectin gel, which reduce the size and inhibits the further growth of the nanoparticles. The shrinked gel was centrifuged and the powder was air dried. The as-prepared composite was further carbonized in Argon atmosphere at 600 °C for 2 h. After annealing, a blackish-white powder was obtained i.e. carbon composite of biosynthesized TiO_2 nanoparticles (Bio-TiO_2/C). For

comparison, bare Bio-TiO_2 was prepared by the same way, except for its annealing in air atmosphere at 600 °C for 2 h. After annealing, a white powder was obtained i.e. biosynthesized TiO_2 nanoparticles (Bio-TiO_2). The role of gram bean extract in this synthesis is to stabilise the Ti ions taking advantage of the biomolecules naturally containing in the extract, which help prevent agglomeration and also serves as natural carbon source forming composite on carbonization in inert environment. The Bio-TiO_2/C and Bio-TiO_2 nanoparticles so produced were further characterized for their structural, morphological and electrochemical properties.

2.3 Structural and morphological characterizations

Thermogravimetric analysis (TGA) was performed using a TA Instruments SDT-Q600 (USA) in the temperature range of 25–900 °C with heating rate of 10 °C min^{-1} in air and argon atmosphere respectively, at flow rate of 20 mL min^{-1}. Powder X-ray diffraction measurement were carried out using Bruker AXS D8 Advance X-ray diffractometer (USA) equipped with Cu $K\alpha_1$ (λ−1.54056 Å) radiation between 10° and 80°. Raman spectrophotometer (STR-150 series, Japan) was used for the analysis of the samples and specifically for identifying the presence of carbon in the composite. FTIR spectra were recorded using FTIR (CARRY 600Z series, Japan) to investigate the characteristic functional groups of the samples. X-ray photoelectron spectroscopy (XPS) analysis was carried out using VG multilab ESCA 2000 system (USA), using a monochromated Mg Kα source (1.254 keV). Morphology of the calcined Bio-TiO_2/C and bare Bio-TiO_2 was observed using transmission electron microscopy (TEM, PHILIPS, CM 200, USA) and selected area electron diffraction (SAED) patterns. Specimens were prepared by ultrasonicating and dispersing Bio-TiO_2/C and bare Bio-TiO_2 in ethanol followed by drop-casting the suspension on a carbon-coated copper grid.

2.4 Electrochemical characterization

Electrochemical studies were carried out in standard two electrode coin-cell (CR 2016) configuration. In electrochemical measurement, metallic lithium was used as both reference and counter electrode. The working/composite electrode was formulated with an accurately weighed 10 mg of active material (Bio-TiO_2/C), 1.5 mg of conductive additive (super P), and 1.5 mg of PVDF as binder. This composite was then pressed under a pressure of 200 kg cm^{-2} on an area of 200 mm^2 onto a stainless steel mesh, which acts as a current collector. This composite electrode was then subsequently dried at 60 °C for 24 h before assembling the coin-cell under an Ar-filled glove box (MBraun, Germany). The electrodes were separated by a microporous glass fiber separator (Whatman, Cat. No. 1825-047, UK) and filled with 1 M $LiPF_6$ in an ethylene carbonate (EC)/diethyl carbonate (DEC) (1: 1 wt%, DAN VEC) mixture as electrolyte. The same procedure was used for the cell fabrication using 10 mg of active material Bio-TiO_2, similar to that used for Bio-TiO_2/C and as discussed earlier. Cyclic voltammetric (CV) traces were recorded using a Solartron 1470E potentiostat in a two electrode configuration at a slow scan rate of 0.1 mV s^{-1}. Galvanostatic cycling profiles were recorded using an Arbin 2000 battery tester at a constant current density of 33 mA g^{-1} between 1 and 3 V for half-cell configurations in ambient temperature conditions.

3 Results and discussion

In situ formation of carbonaceous TiO_2 nanoparticles using the Bengal gram bean extract under different annealing atmosphere were characterized using various analytical techniques for the confirmation of thermal stability, crystal structure, phase purity, elemental analysis and oxidation state. The annealing atmosphere dependent formation of carbonaceous TiO_2 nanoparticles was initially assessed for their decomposition temperature and thermal stability using thermogravimetric analysis (TGA).

3.1 Thermogravimetric analysis (TGA)

TGA thermogravimetric analysis is performed to study the thermal profile and to confirm the formation of carbon in the Bio-TiO_2/C during the calcination of as prepared Bio-TiO_2 in inert atmosphere (argon), in contrary to that calcined in air atmosphere. Figure 1 show comparative TGA thermograms of as prepared bare Bio-TiO_2 (calcined in air

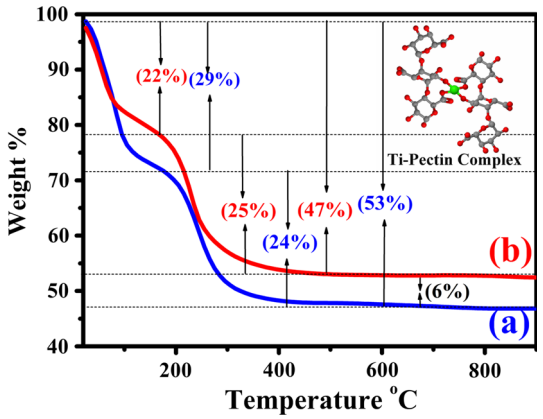

Fig. 1 Representative TG–DTA thermogram of as prepared biosynthesized TiO_2 nanoparticles calcined in air atmosphere (*a*) Bio-TiO_2 (*blue curve*) and in Argon atmosphere (*b*) Bio-TiO_2/C (*red curve*). *Inset* shows Ti-pectin complex (Color figure online)

atmosphere, blue thermogram) and Bio-TiO_2/C (calcined in argon atmosphere, red thermogram). The inset in the figure shows the structure of Ti-pectin complex. The TGA thermogram of as prepared Bio-TiO_2 in air atmosphere shows weight loss in two steps. The first step in the temperature range from 25 to 155 °C shows weight loss of 29 %, which could be attributed to the loss of moisture and water molecules being trapped on or within the surface adsorbed biomolecules of air dried sample. In the second step, 24 % of weight loss is observed in the temperature range from 155 to 430 °C as a result of oxidation and decomposition of surface bound biomolecules during the calcination process. The calcination of Bio-TiO_2 in air atmosphere at 600 °C results in white coloured powder, which indicates the complete oxidation of surface bound biomolecules forming pure TiO_2 nanoparticles. The TGA thermogram of the sample calcined in air atmosphere shows that the mass ratio of TiO_2 to be 47 % TiO_2 plus 53 % of biomolecules and water residues.

On the other hand, the TGA thermogram of as prepared (air dried) Bio-TiO_2 calcined in argon atmosphere shows weight loss in two step. In the first step, weight loss of 22 % is observed in the temperature range from 25 to 165 °C with delayed thermoprofile, probably owing to inert environment. The weight loss in the first step can be attributed to the loss of moisture and water molecules being trapped on or within the surface adsorbed biomolecules of air dried sample. In the second step, in the temperature range from 165 to 450 °C, 25 % weight loss is observed because of the sluggish decomposition/oxidation of surface bound biomolecules. The incomplete decomposition of the biomolecules results in carbonization of biomolecules forming carbon incorporated TiO_2 (Bio-TiO_2/C) [35, 36]. The formation of carbon incorporated TiO_2 (Bio-TiO_2/C) during the calcination of as prepared Bio-TiO_2 in argon atmosphere is due to the deficiency of oxygen in argon atmosphere, which prevents the oxidation of carbon. From the TGA thermogram recorded in argon atmosphere, the mass ratio of Bio-TiO_2 could be estimated at 53 % of carbonized TiO_2 (TiO_2/C) and 47 % of biomolecules and water adsorbed onto the surface. The comparison of the two TGA thermograms clearly reveal difference in weight losses of the samples calcined in air and argon atmosphere and the observed difference in weight loss (6 %) could be attributed to the in situ formed carbonaceous material (decomposition of biomolecules) incorporated in the Bio-TiO_2 sample when calcined in argon atmosphere.

3.2 X-ray diffraction

The crystal phases of the samples are studied by using X-ray diffraction as shown in Fig. 2. The XRD pattern of

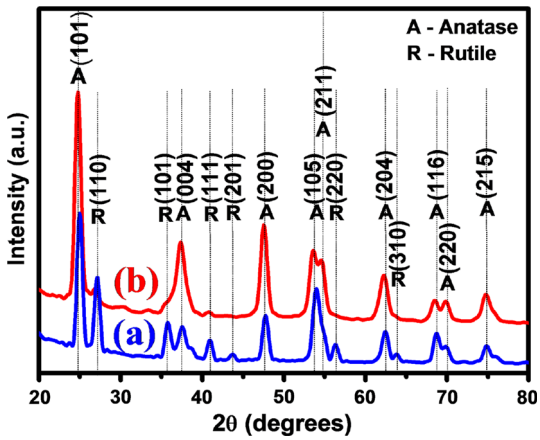

Fig. 2 Representative X-ray diffraction patterns of biosynthesized TiO_2 nanoparticles (*a*) Bio-TiO_2 (*blue spectrum*) and (*b*) Bio-TiO_2/C (*red spectrum*) (Color figure online)

air calcined Bio-TiO_2 sample is composed of anatase (JCPDS, No. 00-002-0387) and rutile (JCPDS, No. 01-076-1938) mixed phases, with anatase being the dominant phase. The anatase and rutile phases belong to space groups $I4_1/amd$ with $Z = 4$ and $P4_2/mnm$ with $Z = 2$, respectively [37]. Crystallite size calculated using Scherrer's equation for anatase and rutile phases are 16 and 21 nm, respectively, with mean crystallite size of 18 nm. The phase fraction by weight determined for bare Bio-TiO_2 is 52.5 % of anatase and 47.5 % of rutile according to the Rietveld Refinement method implemented in Match-2 software. On the other hand, XRD pattern of Bio-TiO_2/C nanoparticles calcined in argon atmosphere, show relatively less intense signal than in case of sample calcined in air. The rutile phase peak in Bio-TiO_2/C is absent, which indicates that the percentage of anatase (JCPDS, No. 00-002-0387) phase in Bio-TiO_2/C is more than in the bare Bio-TiO_2. This could be attributed to the presence of residual surface bound carbon obtained from the decomposition of pectin (biomolecules) in gram bean extract, which remain unburned due to the lack of oxygen [38]. A mean crystallite size of 12 nm is obtained for this sample, which is smaller than the sample calcined in air.

3.3 Raman spectroscopy

Raman spectroscopy is very powerful technique to characterize crystallinity of the material and for phase identification. This technique is also useful to determine the carbon content of the material and thus Raman spectra of both the samples were recorded to confirm the presence of carbon in Bio-TiO_2/C sample. Figure 3 shows the Raman spectra of bare Bio-TiO_2 and Bio-TiO_2/C. Well resolved Raman scattering peaks at 142 (E_g), 196 (E_g), 397(B_{1g}),

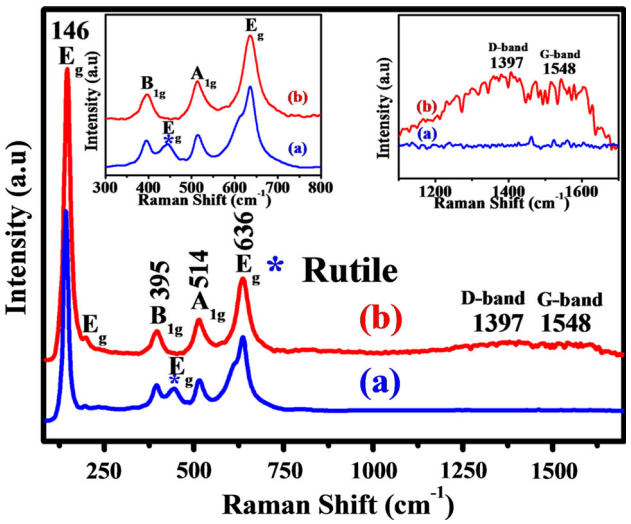

Fig. 3 Representative Raman spectra of biosynthesized TiO_2 nanoparticles (*a*) Bio-TiO_2 (*blue spectrum*) and (*b*) Bio-TiO_2/C (*red spectrum*) (Color figure online)

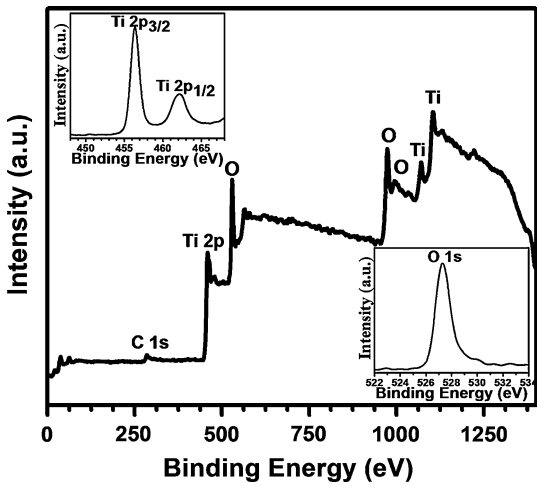

Fig. 4 XPS survey spectrum of biosynthesized TiO_2 nanoparticles and inset shows core level spectra for Ti 2p and O1 s of of biosynthesized TiO_2 nanoparticles

514 (A_{1g}) and 637 cm^{-1} (E_g) characteristic of anatase phase and weak peak located at 446 cm^{-1} characteristic of rutile phase is observed for air calcined Bio-TiO_2 [37]. On the other hand, the spectrum obtained from the sample calcined in argon atmosphere (Bio-TiO_2/C) shows peaks characteristic of anatase phase and no peak at 446 cm^{-1} characteristic of rutile phases is observed. This indicates that only the anatase phase is formed in sample calcined in argon atmosphere (Bio-TiO_2/C). In addition to the peaks originating from anatase phase, additional two less intense peaks at 1397 (D-band) and 1548 cm^{-1} (G-band) were observed indicating the presence of disordered elemental carbon [39]. Based on above characterizations, it can be concluded that the in situ carbon incorporated TiO_2 nanoparticles could be successfully prepared using biosynthesis approach on calcinations in argon atmosphere.

3.4 X-ray photoelectron spectroscopy

Figure 4 shows the representative XPS survey spectra of Bio-TiO_2 confirming the chemical composition, while the insets show core level spectra confirming the chemical states of the Ti and O elements. The core level Ti 2p spectrum (inset in upper left corner) shows two peaks characteristic of Ti $2p_{3/2}$ and Ti $2p_{1/2}$ at 456.3 and 462.1 eV, respectively, which correspond to Ti^{4+} of TiO_2 in the tetragonal structure [40]. Difference between these two peaks is about 5.8 eV, which is in good agreement with the literature report for TiO_2. Furthermore, the core level spectrum of O 1 s (inset in lower right corner) shows peak at 527 eV, which could be ascribed to Ti–O in TiO_2.

3.5 Fourier transform infrared spectroscopy

Figure 5 shows the FT-IR spectra of bare Bio-TiO_2 and Bio-TiO_2/C. As shown in the FTIR spectrum of Bio-TiO_2, the peak at 3230 and 1643 cm^{-1} could be attributed to the O–H stretching vibrations, while the peaks at 2385 and 685 cm^{-1} are related to carbon dioxide and Ti–O–Ti stretching mode, respectively [41, 42]. However, in case of Bio-TiO_2/C spectrum, two extra peak at 2982 and 1384 cm^{-1} owing to the CH stretching and bending modes in CH_2, respectively, were observed [41, 43]. This also indicates the presence of carbon in Bio-TiO_2/C sample.

3.6 Transmission electron microscopy

Transmission electron microscope (TEM) is employed to observe morphology of bare Bio-TiO_2 and Bio-TiO_2/C. Figure 6a (bare Bio-TiO_2) clearly shows uniform size

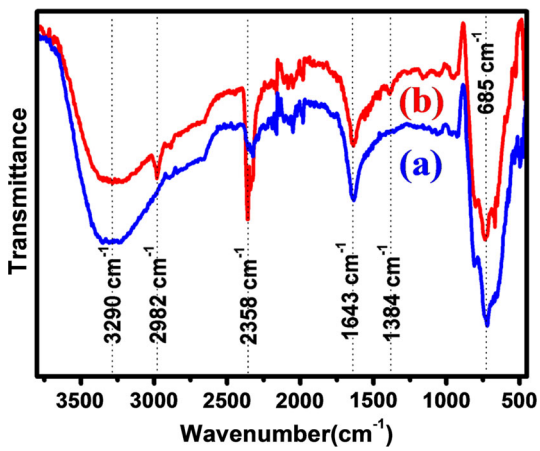

Fig. 5 Representative FTIR of (*a*) Bio-TiO_2 (*blue spectrum*) and (*b*) Bio-TiO_2/C nanoparticles (*red spectrum*) (Color figure online)

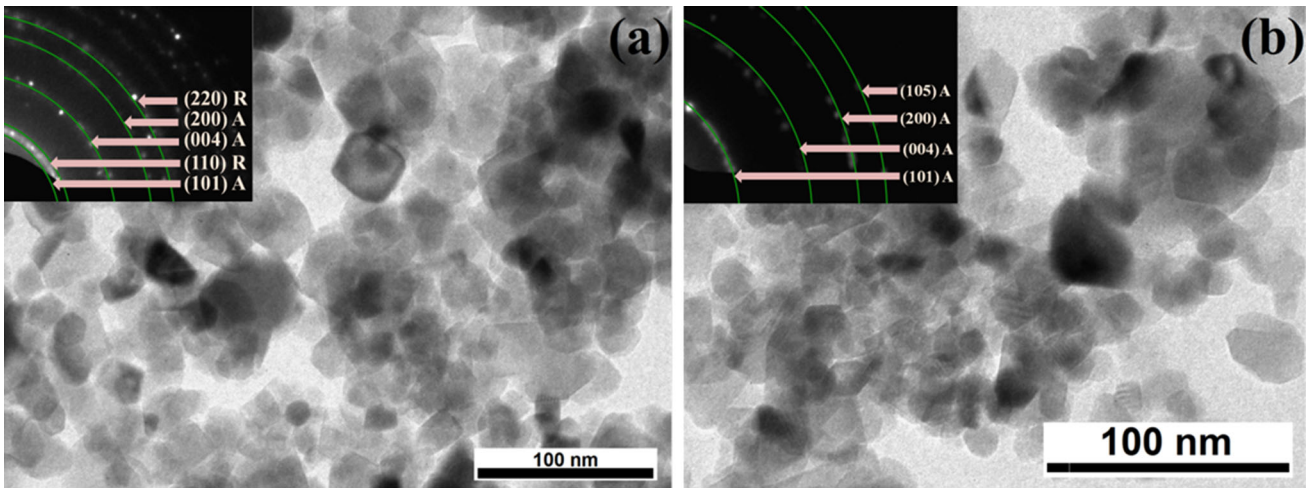

Fig. 6 Representative TEM images of biosynthesized TiO_2 nanoparticles along with their corresponding SAED patterns **a** Bio-TiO_2 and **b** Bio-TiO_2/C nanoparticles

distribution of the roughly spherical Bio-TiO_2 nanoparticles with average size of ~ 18-20 nm. However, the TEM image of Bio-TiO_2/C as in Fig. 6b clearly shows the formation of composite of carbon and TiO_2 with average particle size of ~12–13 nm. The particle size of the both sample noted from TEM is further confirmed through the XRD data by calculating the size using Scherrer's equation. Selected area electron diffraction (SAED) pattern of the bare Bio-TiO_2 is shown as inset in Fig. 6a. The SAED pattern clearly shows bright concentric rings, which were due to the diffraction from the (101), (004) and (200) planes characteristic of anatase phase and (110) and (220) planes for rutile phase, considering the fact that the sample had mixed phases of anatase and rutile TiO_2. This supports the fact that the resulting Bio-TiO_2 consists of mixed phase as confirmed from XRD and Raman study. On the other hand, the SAED pattern of Bio-TiO_2/C (shown as inset in Fig. 6b) clearly shows the diffused ring pattern, which is indicative of polycrystalline nature of Bio-TiO_2/C. The observed diffraction pattern in Bio-TiO_2/C show diffractions from (101), (004), (200) and (105) planes characteristic of anatase phase. Since the sample is calcined in argon atmosphere (Bio-TiO_2/C), it prevents the phase transformation from anatase to rutile even at 600 °C, probably owing to the carbon been capped/covered over TiO_2 nanoparticles. The phase transformation temperature is found to shift to higher temperatures due to the shielding effect of the carbon coating and it is also in good agreement with the XRD and Raman spectrum of Bio-TiO_2/C.

3.7 Electrochemical performance of Bio-TiO_2 and Bio-TiO_2/C

The synthesized bare Bio-TiO_2 and Bio-TiO_2/C samples were explored as electrode for investigating their application in lithium ion battery and for probing the energy storage properties. The electrochemical system consists of half-cell configuration and is operated in the potential range of 1.0–3.0 V at room temperature. The cyclic voltammetry (CV) measurements were recorded and presented in Fig. 7a. The figure shows cyclic voltammograms obtained at the scan rate of 0.1 mV s^{-1} using both bare Bio-TiO_2 and Bio-TiO_2/C based electrode. The materials show redox peak couple at 1.74/1.93 V for Bio-TiO_2/C and at 1.68/1.99 V for bare Bio-TiO_2, which could be attributed to the lithiation and delithiation processes. The obtained results are in good agreement with previous literature report [44]. The Li insertion into anatase TiO_2 is a two phase process, showing co-existence of Li-poor $Li_{0.01}$ TiO_2 and Li-rich $Li_{0.55}$ TiO_2. The CV clearly reveals Bio-TiO_2/C based electrode showing higher current densities than bare Bio-TiO_2 based electrode, which is related to the higher electronic conductivity of Bio-TiO_2/C due to the presence of carbon [27].

The further investigation of Li storage properties were studied by measuring galvanostatic charge–discharge profiles of both bare Bio-TiO_2 and Bio-TiO_2/C. The obtained charge–discharge test results are shown in Fig. 7b. The cell with Bio-TiO_2/C as electrode shows the discharge and charge capacities for the first cycle to be ~208 mA h g^{-1} (0.62 mol of Li) and 197 mA h g^{-1}(0.59 mol of Li), respectively, with columbic efficiency of ~95 % at constant current density of 33 mA g^{-1}. The cell fabricated with bare Bio-TiO_2 exhibits the discharge and charge capacities for the first cycle to be ~199 (0.59 mol of Li) and 185 mA h g^{-1} (0.55 mol of Li), respectively, with columbic efficiency of ~92 % at constant current density of 33 mA g^{-1} corresponding to 0.16 °C current rate. The charge capacity in first cycle of Bio-TiO_2/C is more than the bare Bio-TiO_2, which is due the presence of carbon in

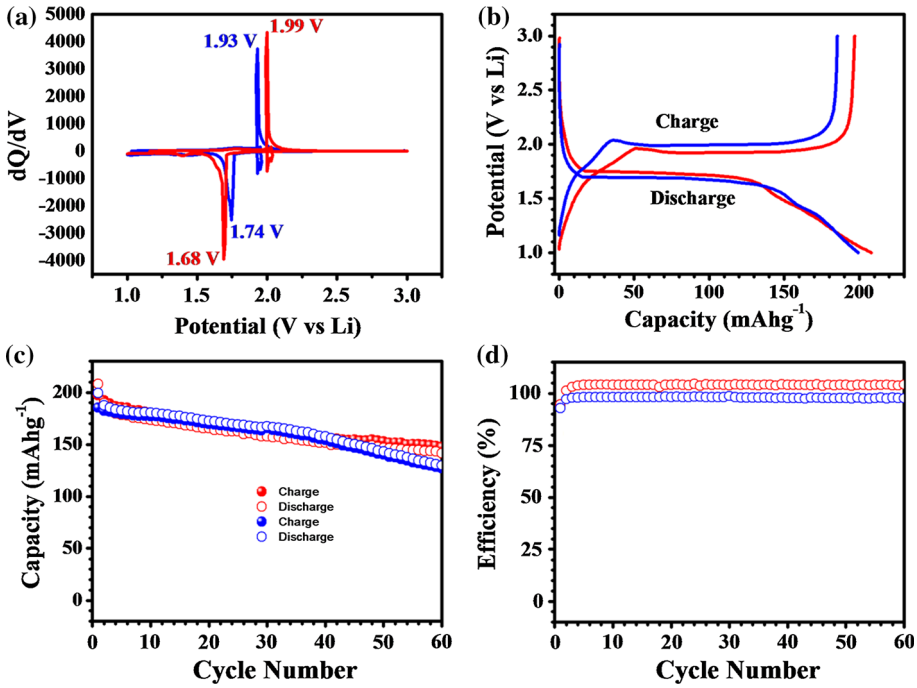

Fig. 7 **a** Cyclic voltammograms (CV) of Bio-TiO_2 (*blue curves*) and Bio-TiO_2/C nanoparticles (*red curves*) half-cell cycle between 1 and 3 V at a scan rate of 0.1 mV s^{-1}, in which, metallic lithium serves as both counter and reference electrode. **b** Initial charge–discharge curves of Li/TiO_2 half-cell cycle between 1 and 3 V at a current density of 33 mA g^{-1} at room temperature. **c** Cycling stability profiles of the Li/TiO_2 cell and **d** Graph showing Coulombic efficiency (%) versus number of cycles (Color figure online)

Bio-TiO_2/C contributing to the increase in conductivity of carbon incorporated Bio-TiO_2 (Bio-TiO_2/C).

Furthermore, to investigate the stability of the electrodes, cycle stability study of the both sample electrodes was performed up to 60 cycles at a current rate of 0.16 °C. Figure 7c clearly shows that the cell delivers more stable cycling profiles with a meagre amount of capacity fading. In bare Bio-TiO_2, the discharging/reversible capacity is more than the Bio-TiO_2/C at a current density of 33 mA g^{-1} during the first 44 cycles (151 mA h g^{-1}). After 44 cycles, the reversible capacity of bare Bio-TiO_2 is observe to fade up to 130 mA h g^{-1} after 60 cycles, while maintaining the CE nearly 97 %. However, in case of Bio-TiO_2/C the trend observed is reverse of bare Bio-TiO_2. The reversible capacity after 44 cycle is constant and more than the bare Bio-TiO_2 and is about 145 mA h g^{-1} after 60 cycles, while maintaining CE nearly 100 %. The capacity in Bio-TiO_2/C is more than bare Bio-TiO_2 due to the connection between the incorporated carbon and TiO_2, which help to increase the conductivity and stability of TiO_2.

4 Conclusions

In summary, we have successfully synthesized carbon incorporated biosynthesized TiO_2 (Bio-TiO_2/C) nanoparticles using simple low cost Bengal gram bean extract medium. The synthesized TiO_2 nanoparticles (Bio-TiO_2/C and bare Bio-TiO_2) were also explored as electrode material in lithium ion battery. The Bio-TiO_2/C shows good electrochemical properties by delivering maximum (208 mA h g^{-1}) discharge capacity and 100 % columbic efficiency over 60 cycles. The obtained results are higher than those obtained from the bare Bio-TiO_2 nanoparticles showing maximum of (197 mA h g^{-1}) discharge capacity and 97 % columbic efficiency over 60 cycles. This confirms that the carbonaceous matter present in Bio-TiO_2/C nanoparticles sample calcined in argon atmosphere is responsible for the improvement of the overall electrochemical properties. This work paves new avenues for the scientific community to develop environmentally benign in situ carbon incorporated TiO_2 nanoparticles using Bengal gram bean extract a green nanotechnology approach.

Acknowledgments A. A. K thanks CSIR, New Delhi, for a research fellowship (File No. 09/809(0013)/2012-EMR-I). The authors are thankful to UGC-DAE Consortium for Scientific Research, Indore (Project Ref. No: CSR-I/CRS-48/48) and UGC, New Delhi (F. No. 41-370/2012 (SR)) for the financial support. Financial support by Ministry of Science and Technology, R.O.C. Contract No. MOST 105-2119-M-011-002 is acknowledged.

References

1. E.C. Evarts, Nature **526**, S93–S95 (2015)
2. M. Armand, J.M. Tarascon, Nature **451**, 652–657 (2008)
3. S.-Z. Huang, Y. Cai, J. Jin, J. Liu, Y. Li, Y. Yu, H.-E. Wang, L.-H. Chen, B.-L. Su, Nano Energy **12**, 833–844 (2015)
4. L. Qin, S. Liang, A. Pan, X. Tan, Mater. Lett. **164**, 44–47 (2016)
5. L. Jabbour, M. Destro, D. Chaussy, C. Gerbaldi, S. Bodoardo, N. Penazzi, D. Beneventi, Compos. Sci. Technol. **87**, 232–239 (2013)
6. N.A. Garcia-Gomez, D.I. Garcia-Gutierrez, S. Sepulveda-Guzman, E.M. Sanchez, J. Mater. Sci.: Mater. Electron. **24**, 3976–3984 (2013)

7. G.C. Chung, S.H. Jun, K.Y. Lee, M.H. Kim, J. Electrochem. Soc. **146**, 1664–1671 (1999)
8. N. Loeffler, D. Bresser, S. Passerini, M. Copley, Johns. Matthey Technol. Rev. **59**, 34–44 (2015)
9. R. Yazami, Electrochim. Acta **45**, 87–97 (1999)
10. H. Liu, D. Long, X. Liu, W. Qiao, L. Zhan, L. Ling, Electrochim. Acta **54**, 5782–5788 (2009)
11. H. Liu, J. Chen, R. Hu, X. Yang, H. Ruan, Y. Su, W. Xiao, J. Mater. Sci.: Mater. Electron. **27**, 3968–3973 (2016)
12. Z. Ma, H. Zhang, Y. Zhang, J. Zhang, Z. Li, Electrochim. Acta **176**, 1427–1433 (2015)
13. F. Zheng, S. Xu, Y. Zhang, J. Mater. Sci.: Mater. Electron. **27**, 3576–3582 (2016)
14. Y. Zhang, Y. Wu, Y. Chu, L. Li, Q. Yu, Y. Zhu, G. Liu, Q. Hou, R. Zeng, L. Zhao, Electrochim. Acta **188**, 909–916 (2016)
15. M.M. Vadiyar, S.C. Bhise, S.S. Kolekar, J.-Y. Chang, K.S. Ghule, A.V. Ghule, J. Mater. Chem. A **4**, 3504–3512 (2016)
16. Y. Jiang, D. Zhang, Y. Li, T. Yuan, N. Bahlawane, C. Liang, W. Sun, Y. Lu, M. Yan, Nano Energy **4**, 23–30 (2014)
17. A.A. Voskanyan, C.-Y.V. Li, K.-Y. Chan, L. Gao, CrystEngComm **17**, 2620–2623 (2015)
18. X.-Y. Yu, H.B. Wu, L. Yu, F.-X. Ma, X.W. Lou, Angew. Chem. Int. Ed. **54**, 4001–4004 (2015)
19. J. Chen, H. Hou, Y. Yang, W. Song, Y. Zhang, X. Yang, Q. Lan, X. Ji, Electrochim. Acta **164**, 330–336 (2015)
20. L. Kavan, J. Solid State Electrochem. **18**, 2297–2306 (2014)
21. M.M. Rahman, J.-Z. Wang, M.F. Hassan, D. Wexler, H.K. Liu, Adv. Energy Mater. **1**, 212–220 (2011)
22. H. Lin, X. Li, X. He, J. Zhao, Electrochim. Acta **173**, 242–251 (2015)
23. X. Zhang, V. Aravindan, S. Madhavi, J. Phys. Chem. C **116**, 14780 (2012)
24. T. Tao, L. He, J. Li, Y. Zhang, J. Alloys Compd. **615**, 1052–1055 (2014)
25. Y. Liu, Y. Yang, J. Nanomater. **2016**, 8123652 (2016)
26. X. Yan, Z. Wang, M. He, Z. Hou, T. Xia, G. Liu, X. Chen, Energy Technol. **3**, 801–814 (2015)
27. S. Goriparti, E. Miele, M. Prato, A. Scarpellini, S. Marras, S. Monaco, A. Toma, G.C. Messina, A. Alabastri, F.D. Angelis, L. Manna, C. Capiglia, R.P. Zaccaria, ACS Appl. Mater. Interfac **7**, 25139–25146 (2015)
28. Y. Chen, X. Ma, X. Cui, Z. Jiang, J. Power Sources **302**, 233–239 (2016)
29. Q. Wang, Z.H. Wen, J.H. Li, Adv. Funct. Mater. **16**, 2141–2146 (2006)
30. M. Dahl, Y. Liu, Y. Yin, Chem. Rev. **114**, 9853–9889 (2014)
31. P. Acevedo-Peña, M.E. Rincón, J. Mater. Sci.: Mater. Electron. **27**, 2985–2993 (2016)
32. K.P. Gattu, K. Ghule, A.A. Kashale, A.V. Ghule, RSC Adv. **5**, 72849 (2015)
33. K.P. Gattu, K. Ghule, A.A. Kashale, A.V. Ghule, Curr Nanosci **11**, 253–260 (2015)
34. A.A. Kashale, K.P. Gattu, K. Ghule, V.H. Ingole, S. Dhanayat, R. Sharma, J.-Y. Chang, A.V. Ghule, Compos Part B **99**, 297–304 (2016)
35. A. Henry, S. Plumejeau, L. Heux, N. Louvain, L. Monconduit, L. Stievano, B. Boury, ACS Appl. Mater. Interfaces **7**, 14584–14592 (2015)
36. K.A. Saharudin, S. Sreekantan, C.W. Lai, Mater. Sci. Semicond. Process. **20**, 1–6 (2014)
37. J. Shen, L. Wang, RSC Adv. **2**, 9173 (2012)
38. M. Inagaki, F. Kojin, B. Tryba, M. Toyoda, Carbon **43**, 1652–1659 (2005)
39. M.-H. Ryu, K.-N. Jung, K.-H. Shin, K.-S. Han, S. Yoon, J. Phys. Chem. C **117**, 8092–8098 (2013)
40. Y.F. Wang, L.P. Li, X.S. Huang, Q. Li, G.S. Li, RSC Adv. **5**, 34302–34313 (2015)
41. S.S. Mali, C.A. Betty, P.N. Bhosale, P.S. Patil, ECS J. Solid State Sci. Technol. **1**, M15–M23 (2012)
42. J.-H. Jeong, D.-W. Jung, E.W. Shin, E.-S. Oh, J. Alloys Compd. **604**, 226–232 (2014)
43. D. Sun, J. Yang, X. Wang, Nanoscale **2**, 287–292 (2010)
44. J. Brumbarov, J.P. Vivek, S. Leonardi, C. Valero-Vidal, E. Portenkirchner, J. Kunze-Liebhauser, J. Mater. Chem. A **3**, 16469–16477 (2015)